Twice-enhanced quantum entanglement in a dual-coupled auxiliary-sphere-assisted cavity magnomechanical system

Zhi-Qiang Liu,[1] Jie Liu,[1] Lei Tan,[1,2,*] and Wu-Ming Liu[3,†]

[1]*Lanzhou Center for Theoretical Physics, Key Laboratory of Theoretical Physics of Gansu Province, and Key Laboratory of Quantum Theory and Applications of MOE, Lanzhou University, Lanzhou, Gansu 730000, China*

[2]*Key Laboratory for Magnetism and Magnetic Materials of the Ministry of Education, Lanzhou University, Lanzhou 730000, China*

[3]*Beijing National Laboratory for Condensed Matter Physics, Institute of Physics, Chinese Academy of Sciences, Beijing 100190, China*

(Received 28 January 2024; accepted 19 July 2024; published 5 August 2024)

We propose a mechanism to significantly enhance the photon-phonon entanglement twice by coupling an auxiliary magnetic sphere to a standard cavity magnomechanical system. The deformed sphere acts as a cold reservoir that can simultaneously cool two hybrid modes superposed over the optical cavity and the mechanical oscillator by modulating the relationship between the coupling strengths, which enables us to obtain large steady-state cavity-oscillator entanglement. On the basis of the double-mode cooling effect, the steady-state photon-phonon entanglement can be significantly improved by opening the single-coupled auxiliary-sphere-assisted channel due to the fact that the nonsuperposed optical mode can be efficiently cooled via the auxiliary sphere. More importantly, the photon-phonon entanglement can be significantly enhanced again by switching the dual-coupled auxiliary-sphere-assisted (DC-ASA) passage, where the auxiliary sphere serves as an additional cold bath to simultaneously cool both the nonsuperposed optical mode and the reservoir mode. Moreover, in the DC-ASA regime, the steady-state entanglement is more robust against the mechanical thermal noise. This DC-ASA scheme can be potentially applied to accelerate magnomechanical cooling and enhance magnomechanical squeezing.

DOI: 10.1103/PhysRevA.110.023707

I. INTRODUCTION

In the past few decades, among ferromagnetic materials, the yttrium iron garnet (YIG) sphere has especially been widely used in various fields because it has the excellent properties of a low dissipation rate and high spin density [1–3]. The magnon (the quanta of collective spin excitations) in the YIG can be coherently coupled with optical and microwave photons, as well as with phonons via magneto-optical effects [4–11], magnetic dipole interactions [12–16], and magnetostrictive forces [17,18], which induces three branches of quantum optics, namely, cavity optomagnonics, cavity electromagnonics, and cavity magnomechanics. These magnon-based hybrid systems provide promising platforms for the study of novel quantum phenomena, such as magnomechanically induced transparency [19,20], bistability [21], magnon dark modes [22], nonreciprocity [23–25], the magnon Kerr effect [26,27], slow light [28–30], the magnon blockade [31–36], and so on.

In particular, in an initial work, the magnon-photon-phonon tripartite entanglement was realized in a standard cavity magnomechanical system [18]. This opened the door to the development of quantum correlations. Subsequently, various coupling schemes based on hybrid cavity-magnon systems have been proposed to generate quantum cooling [37–40], quantum coherence [41], quantum steering [42], quantum squeezing [43–45], etc. Moreover, quantum entanglement has attracted considerable attention as an indispensable ingredient for quantum information processing. Recently, the steady-state entanglement between different degrees of freedom, including photons, phonons, magnons, and atoms, has been extensively studied through a large number of cavity magnomechanical theory schemes [18,26,31,41,42,46–56]. However, entanglement as a fragile quantum resource is highly susceptible to environmental thermal noise. Therefore, to observe quantum entanglement under more demanding experimental conditions, various methods have been proposed to enhance entanglement and its robustness against temperature, such as the reservoir-engineering approach [57], optical-parametric-amplifier scheme [58], auxiliary-microwave-cavity-assisted method [59], coherent-feedback-loop mechanism [60], and so on. The reservoir-engineering scheme can significantly enhance entanglement, although it has higher requirements for experimental parameters. Several other approaches are feasible with experimentally tractable parameters but do not severely enhance entanglement. Thus, exploring a perfect scheme to improve entanglement is an urgent task in cavity magnomechanics.

In this paper, inspired by the auxiliary-cavity-assisted mechanism [59,61,62], we propose a dual-coupled auxiliary-sphere-assisted (DC-ASA) approach to significantly enhance the photon-phonon entanglement with experimentally feasible parameters. We design a hybrid cavity-magnon device consisting of a standard cavity magnomechanical system and

*Contact author: tanlei@lzu.edu.cn
†Contact author: wliu@iphy.ac.cn

an auxiliary YIG sphere. The standard cavity magnomechanical system can interact with the auxiliary sphere via magnon-photon and magnon-magnon couplings, where the magnon-magnon dipolelike interaction strength is tunable through the distance between the two spheres [63]. Inside a standard magnomechanical cavity, the magnon mode is directly coupled to the optical mode via magnetic dipole interaction and parametrically coupled to the mechanical mode by the magnetostrictive effect [18]. By optimizing the relationship between the magnetic dipole and magnetostrictive interaction strengths, we achieve simultaneous cooling of a pair of superposed modes with a common reservoir mode. This is beneficial for the cooling of the system and for the entanglement between the cavity and the oscillator. In the double-mode cooling parameter regime, one of the components of the superposed mode, the optical mode, can be cooled directly by opening a single magnon-photon coupling channel between the auxiliary sphere and the standard system. This motivates us to enhance the photon-phonon entanglement with the single-coupled auxiliary-sphere-assisted (SC-ASA) mechanism. Interestingly, when we simultaneously open the dual magnon-photon and magnon-magnon coupling passages between the auxiliary sphere and the standard system, the photon-phonon entanglement can be further significantly enhanced, which is not possible with the single-coupled auxiliary-cavity-assisted scheme [59,61,62]. This is due to the fact that not only the nonsuperposed optical mode but also the reservoir mode can be efficiently cooled by the auxiliary sphere using the DC-ASA method. Furthermore, the robustness of entanglement against temperature can also be dramatically enhanced, which provides a viable way to protect fragile quantum resources. The main innovations are briefly summarized in our work as follows: (1) The double-mode cooling effect is achieved by optimizing the ratio of the magnetic dipole and magnetostrictive interaction strengths. (2) In the two-mode cooling regime, the cavity-oscillator entanglement can be sharply enhanced by opening the SC-ASA channel between the auxiliary sphere and the standard magnomechanical system. (3) The photon-phonon entanglement can be significantly improved again by switching the DC-ASA passage on the basis of the SC-ASA mechanism, and (4) the cavity-mechanical entanglement is also more robust against environmental thermal perturbations when the system operates in the DC-ASA regime.

The rest of this paper is organized as follows. In Sec. II, we give the cavity magnomechanical model and Hamiltonian for the SC-ASA and DC-ASA systems. In Sec. III, we study the steady-state dynamics of the system, derive the linearized Hamiltonian for our physical model using the quantum Langevin equations (QLEs), and quantify the bipartite entanglement via the logarithmic negativity. In Sec. IV, using the double-mode cooling effect, we discuss the cooling of the system and steady-state photon-phonon entanglement with numerical results in both the SC-ASA and DC-ASA regimes. Finally, the conclusion is presented in Sec. V.

II. MODEL AND HAMILTONIAN

To significantly enhance quantum entanglement we propose to construct a coupled four-mode bosonic system, where the Hamiltonian of this system is given by ($\hbar = 1$)

$$\begin{aligned} H_{\rm dc} =& \omega_a a^\dagger a + \omega_1 m_1^\dagger m_1 + \omega_2 m_2^\dagger m_2 + \omega_b b^\dagger b \\ &+ G_{am}(a m_1^\dagger + a^\dagger m_1) + J_1(a m_2^\dagger + a^\dagger m_2) \\ &+ G_{bm}^0 m_1^\dagger m_1 (b + b^\dagger) + J_2(m_1^\dagger m_2 + m_1 m_2^\dagger) \\ &+ i\varepsilon\left(m_1^\dagger e^{-i\omega_d t} - m_1 e^{i\omega_d t}\right). \end{aligned} \tag{1}$$

Here, the bosonic mode m_2 acts as an auxiliary subsystem realizing dual coupling with the main system via the interactions J_1 and J_2. The single-coupling auxiliary mechanism can be applied to enhance entanglement and cooling, which was already demonstrated in optomechanical and magnomechanical systems [59,61,62]. Therefore, we believe that we can find more interesting phenomena in a dual-coupled auxiliary system. Next, we will confirm our idea by comparing the single-coupling and dual-coupling mechanisms.

A. SC-ASA model and Hamiltonian

First, we consider the case of $J_2 = 0$ in Eq. (1), i.e., the single-coupled auxiliary mechanism. To construct such a device, we focus on cavity magnomechanical platforms which recently attracted wide interest.

As a representative, we envision a SC-ASA hybrid magnomechanical system, where an auxiliary YIG sphere is coupled to a standard cavity magnomechanical system only by the magnon-photon interaction J_1, as shown in Fig. 1(b). Inside the standard system, the deformed sphere m_1 is coupled to the mechanical mode b by magnetostrictive interaction and to the microwave cavity a via magnetic dipole interaction. Discarding the interaction $J_2(m_1^\dagger m_2 + m_1 m_2^\dagger)$ in Eq. (1), this is the Hamiltonian of the SC-ASA system. For the SC-ASA Hamiltonian, a, m_j ($j = 1, 2$), and b are the annihilation operators of the microwave-field (frequency ω_a), jth magnon (frequency ω_j), and vibrational (frequency ω_b) modes, respectively. And the frequency ω_j of the jth magnon mode is defined as $\omega_j = \eta H_j$, where $\eta/2\pi = 28$ GHz/T is the gyromagnetic ratio and H_j is the bias magnetic field of the jth YIG sphere. G_{am} is the coupling strength between the deformed sphere m_1 and the cavity field a. The J_1 term is the single coupling (with strength J_1) between the auxiliary sphere m_2 and the magnomechanical cavity a. $G_{bm}^0 m_1^\dagger m_1 (b + b^\dagger)$ describes the magnomechanical interaction between the magnon mode m_1 and the mechanical mode b with a single-magnon weak-coupling rate G_{bm}^0. The last term in Eq. (1) indicates that the magnon mode m_1 is directly driven by a microwave source with frequency ω_d and driving strength ε. The Rabi frequency ε is defined as $\varepsilon = \frac{\sqrt{5}}{4}\eta\sqrt{N}B_0$, where B_0 is the amplitude of the driving source and $N = \rho V$ is the total number of spins, with $\rho = 4.22 \times 10^{27}$ m^{-3} being the spin density of the YIG and V being the volume of the sphere.

Then the SC-ASA Hamiltonian, in the rotating frame with respect to the laser driving frequency ω_d, can be expressed as

$$\begin{aligned} H_{\rm sc}^{\rm rot} =& \Delta_a a^\dagger a + \Delta_1' m_1^\dagger m_1 + \Delta_2 m_2^\dagger m_2 + \omega_b b^\dagger b \\ &+ G_{am}(a m_1^\dagger + a^\dagger m_1) + J_1(a m_2^\dagger + a^\dagger m_2) \\ &+ G_{bm}^0 m_1^\dagger m_1 (b + b^\dagger) + i\varepsilon(m_1^\dagger - m_1), \end{aligned} \tag{2}$$

where $\Delta_a = \omega_a - \omega_d$, $\Delta_1' = \omega_1 - \omega_d$, and $\Delta_2 = \omega_2 - \omega_d$ are the corresponding detunings.

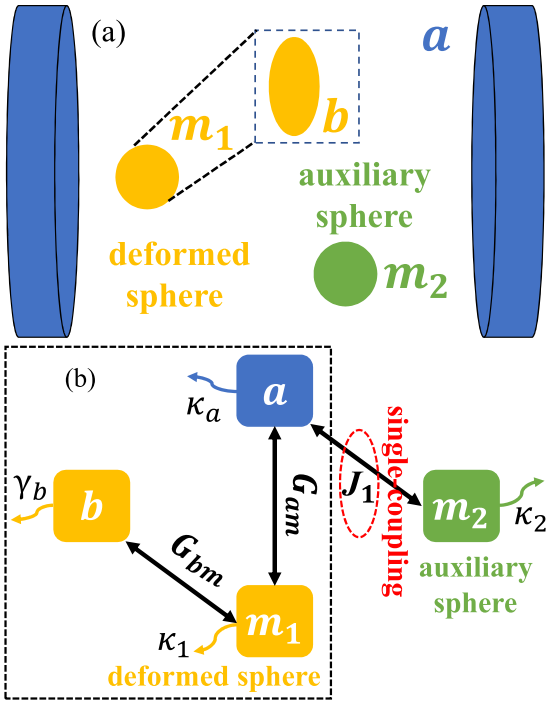

FIG. 1. (a) Schematic of a hybrid cavity magnomechanical device. The auxiliary sphere is placed in a standard cavity magnomechanical system consisting of a deformed sphere and a microwave cavity. The deformed sphere is driven directly by an additional microwave source, which induces a mechanical oscillator. (b) Theoretical model of the SC-ASA magnomechanical system. A standard cavity magnomechanical system is shown in the dashed box. The magnon mode m_1 interacts with the mechanical mode b (the cavity mode a) via the magnomechanical coupling G_{bm} (the magnetic dipole coupling G_{am}). The auxiliary magnon mode m_2 interacts with the standard magnomechanical system via a single coupling J_1.

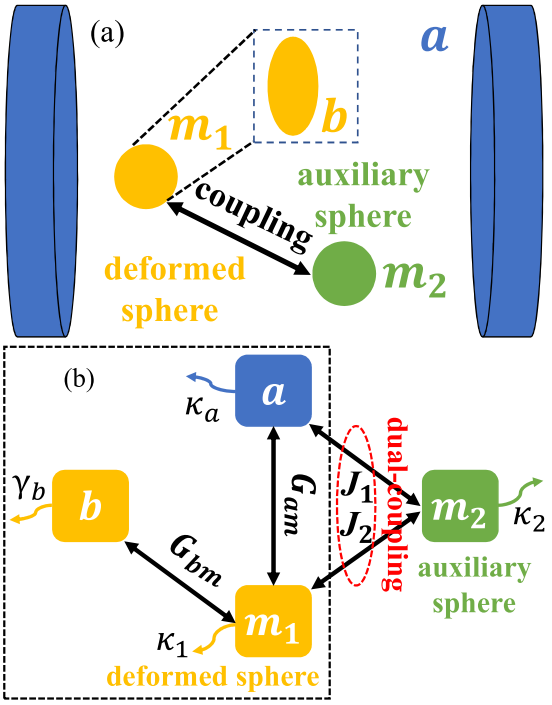

FIG. 2. (a) Sketch of a coupled cavity magnomechanical setup. A deformed YIG sphere and an auxiliary YIG sphere are placed in a microwave cavity, which is the same as in Fig. 1(a). However, here, we consider the coupling between the deformed sphere and the auxiliary sphere compared to Fig. 1(a). (b) Theoretical model of the DC-ASA magnomechanical scheme. The dashed box represents a standard cavity magnomechanical system. The auxiliary magnon mode m_2 interacts with the typical cavity magnomechanical system via dual coupling J_1 and J_2. Here, J_2 describes the dipole-like interaction between the deformed magnon m_1 and the auxiliary magnon m_2.

B. DC-ASA model and Hamiltonian

Now, we consider the case of $J_2 \neq 0$ in Eq. (1), which can be obtained by adjusting the distance between the two YIG spheres in the microwave cavity in Fig. 1(a). The DC-ASA model as displayed in Fig. 2 matches the Hamiltonian (1) that we aspired to realize at the beginning of the article perfectly. The J_2 term in the DC-ASA Hamiltonian (1) symbolizes the beam-splitter-like interaction between the two magnetostatic modes m_1 and m_2, for which the coupling strength J_2 enters the strong-coupling regime when the distance between the two YIG spheres is smaller than their diameter [63].

Up to now, we have constructed the SC-ASA and DC-ASA systems by simply engineering an auxiliary YIG sphere. Next, we will discuss the steady-state dynamics and bipartite entanglement in these two regimes in detail.

III. STATIONARY DYNAMICS

In this section, we investigate the steady-state dynamics of the system by means of the QLEs and linearization techniques and quantify two-body entanglement through the logarithmic negativity in the SC-ASA and DC-ASA mechanisms.

A. SC-ASA system dynamics

It is well known that an imperfect open quantum system is susceptible to decay and ambient noise. Therefore, under the Markovian approximation, the dynamical evolution of the system can be described by the QLEs as follows:

$$\begin{aligned}
\dot{a} &= -i\Delta_a a - iG_{am}m_1 - iJ_1 m_2 - \kappa_a a + \sqrt{2\kappa_a}a_{\rm in},\\
\dot{m}_1 &= -i\Delta_1' m_1 - iG_{am}a - iG_{bm}^0(b+b^\dagger)m_1 + \varepsilon\\
&\quad - \kappa_1 m_1 + \sqrt{2\kappa_1}m_1^{\rm in},\\
\dot{m}_2 &= -i\Delta_2 m_2 - iJ_1 a - \kappa_2 m_2 + \sqrt{2\kappa_2}m_2^{\rm in},\\
\dot{b} &= -i\omega_b b - iG_{bm}^0 m_1^\dagger m_1 - \gamma_b b + \sqrt{2\gamma_b}b_{\rm in},
\end{aligned} \tag{3}$$

where κ_a, κ_1, and κ_2 are the dissipation rates of the microwave cavity, deformed sphere, and auxiliary sphere, respectively, and γ_b is the damping of the mechanical resonator. $a_{\rm in}$, $m_j^{\rm in}$, and $b_{\rm in}$ are input quantum noises for the photon, jth magnon, and phonon modes, respectively. We consider the case where the optical mode and the jth magnon mode are coupled to a vacuum reservoir and the mechanical mode is subjected to a thermal environment. In this case, these noise operators have zero mean values and

follow the following nonzero correlation functions ($j = 1, 2$):

$$\begin{aligned}\langle a_{\rm in}(t)a_{\rm in}^{\dagger}(t')\rangle &= \delta(t-t'),\\ \left\langle m_j^{\rm in}(t)m_j^{in,\dagger}(t')\right\rangle &= \delta(t-t'),\\ \langle b_{\rm in}(t)b_{\rm in}^{\dagger}(t')\rangle &= (\overline{n}_b+1)\delta(t-t'),\\ \langle b_{\rm in}^{\dagger}(t)b_{\rm in}(t')\rangle &= \overline{n}_b\delta(t-t').\end{aligned} \tag{4}$$

Here, the mean thermal excitation number of the mechanical oscillator is given by $\overline{n}_b = [\exp(\hbar\omega_b/k_BT)-1]^{-1}$, where k_B is the Boltzmann constant and T is the bath temperature. In the high-temperature limit, the excitation number $\overline{n}_b \simeq k_BT/\hbar\omega_b$.

When the deformed sphere m_1 is driven strongly, the classical mean value of each bosonic mode is much larger than the quantum fluctuation, which leads to nonlinear effects in the system. To eliminate the nonlinear terms in the Hamiltonian, we rewrite each Heisenberg operator in Eq. (3) as the sum of the steady-state amplitude and the additional fluctuation, $a = \alpha + \delta a$, $m_j = \chi_j + \delta m_j$, and $b = \beta + \delta b$, with $|\alpha|, |\chi_j| \gg 1$ and $\langle \delta O\rangle = \langle \delta m_j\rangle = 0$ ($O = a, b$). By studying the evolution of the classical amplitudes and the quantum fluctuations separately, we obtain a set of equations for the steady-state averages,

$$\begin{aligned}\dot{\alpha} &= -i\Delta_a\alpha - iG_{am}\chi_1 - iJ_1\chi_2 - \kappa_a\alpha,\\ \dot{\chi}_1 &= -i\Delta_1\chi_1 - iG_{am}\alpha + \varepsilon - \kappa_1\chi_1,\\ \dot{\chi}_2 &= -i\Delta_2\chi_2 - iJ_1\alpha - \kappa_2\chi_2,\\ \dot{\beta} &= -i\omega_b\beta - iG_{bm}^0|\chi_1|^2 - \gamma_b\beta,\end{aligned} \tag{5}$$

and a set of linearized QLEs for the additional fluctuations,

$$\begin{aligned}\delta\dot{a} =& -i\Delta_a\delta a - iG_{am}\delta m_1 - iJ_1\delta m_2 - \kappa_a\delta a + \sqrt{2\kappa_a}a_{\rm in},\\ \delta\dot{m}_1 =& -i\Delta_1\delta m_1 - iG_{am}\delta a - iG_{bm}^0\chi_1(\delta b + \delta b^{\dagger})\\ & - \kappa_1\delta m_1 + \sqrt{2\kappa_1}m_1^{\rm in},\\ \delta\dot{m}_2 =& -i\Delta_2\delta m_2 - iJ_1\delta a - \kappa_2\delta m_2 + \sqrt{2\kappa_2}m_2^{\rm in},\\ \delta\dot{b} =& -i\omega_b\delta b - iG_{bm}^0(\chi_1^*\delta m_1 + \chi_1\delta m_1^{\dagger}) - \gamma_b\delta b + \sqrt{2\gamma_b}b_{\rm in},\end{aligned} \tag{6}$$

where $\Delta_1 = \Delta_1' + G_{bm}^0(\beta+\beta^*)$ is the normalized detuning of the deformed sphere. In the linearization process, we reasonably omit the higher-order nonlinear terms. Conversely, starting from Eq. (6), we can obtain the linearized Hamiltonian of the SC-ASA system for the fluctuation operators,

$$\begin{aligned}H_{\rm sc}^{\rm lin} =& \Delta_a\delta a^{\dagger}\delta a + \Delta_1\delta m_1^{\dagger}\delta m_1 + \Delta_2\delta m_2^{\dagger}\delta m_2 + \omega_b\delta b^{\dagger}\delta b\\ &+ G_{am}(\delta a^{\dagger}\delta m_1 + \delta a\delta m_1^{\dagger}) + J_1(\delta a^{\dagger}\delta m_2 + \delta a\delta m_2^{\dagger})\\ &+ [G_{bm}(\delta m_1^{\dagger}\delta b + \delta m_1\delta b) + \text{H.c.}],\end{aligned} \tag{7}$$

where $G_{bm} = G_{bm}^0\chi_1$ is the effective magnomechanical coupling strength. Without loss of generality, we assume that G_{bm} is a positive real number.

Now, we define a column vector $U = [\delta x_a, \delta y_a, \delta x_1, \delta y_1, \delta x_2, \delta y_2, \delta q, \delta p]^T$ consisting of a set of quadrature operators which can be represented by all the quantum fluctuation operators of the system, where $\delta x_a = (\delta a + \delta a^{\dagger})/\sqrt{2}$, $\delta x_j = (\delta m_j + \delta m_j^{\dagger})/\sqrt{2}$, and $\delta q = (\delta b + \delta b^{\dagger})/\sqrt{2}$ are quadrature position operators and $\delta y_a = (\delta a - \delta a^{\dagger})/i\sqrt{2}$, $\delta y_j = (\delta m_j - \delta m_j^{\dagger})/i\sqrt{2}$, and $\delta p = (\delta b - \delta b^{\dagger})/i\sqrt{2}$ are quadrature momentum operators ($j = 1, 2$). Then, the linearized QLEs for the small fluctuations in Eq. (6) can be expressed by the quadrature operators as

$$\dot{U} = M_{\rm sc}U + N, \tag{8}$$

where the coefficient matrix $M_{\rm sc}$ is given by

$$M_{\rm sc} = \begin{pmatrix} -\kappa_a & \Delta_a & 0 & G_{am} & 0 & J_1 & 0 & 0\\ -\Delta_a & -\kappa_a & -G_{am} & 0 & -J_1 & 0 & 0 & 0\\ 0 & G_{am} & -\kappa_1 & \Delta_1 & 0 & 0 & 0 & 0\\ -G_{am} & 0 & -\Delta_1 & -\kappa_1 & 0 & 0 & -2G_{bm} & 0\\ 0 & J_1 & 0 & 0 & -\kappa_2 & \Delta_2 & 0 & 0\\ -J_1 & 0 & 0 & 0 & -\Delta_2 & -\kappa_2 & 0 & 0\\ 0 & 0 & 0 & 0 & 0 & 0 & -\gamma_b & \omega_b\\ 0 & 0 & -2G_{bm} & 0 & 0 & 0 & -\omega_b & -\gamma_b \end{pmatrix}$$

and $N = [\sqrt{2\kappa_a}X_a^{\rm in}, \sqrt{2\kappa_a}Y_a^{\rm in}, \sqrt{2\kappa_1}X_1^{\rm in}, \sqrt{2\kappa_1}Y_1^{\rm in}, \sqrt{2\kappa_2}X_2^{\rm in}, \sqrt{2\kappa_2}Y_2^{\rm in}, \sqrt{2\gamma_b}Q^{\rm in}, \sqrt{2\gamma_b}P^{\rm in}]^T$ is the vector of input noises. The Hermitian noise operators have forms similar to the quadrature operators, $X_a^{\rm in} = (a_{\rm in} + a_{\rm in}^{\dagger})/\sqrt{2}$, $Y_a^{\rm in} = (a_{\rm in} - a_{\rm in}^{\dagger})/i\sqrt{2}$, $X_j^{\rm in} = (m_j^{\rm in} + m_j^{in,\dagger})/\sqrt{2}$, $Y_j^{\rm in} = (m_j^{\rm in} - m_j^{in,\dagger})/i\sqrt{2}$, $Q^{\rm in} = (b_{\rm in} + b_{\rm in}^{\dagger})/\sqrt{2}$, and $P^{\rm in} = (b_{\rm in} - b_{\rm in}^{\dagger})/i\sqrt{2}$. After performing the above quadrature transformation, the dynamics of the system are always linearized, and the ambient noise is Gaussian, so the relevant quantum properties of the continuous variable system can be described by the symmetric 8×8 covariance matrix $\Theta_{\rm sc}$ with matrix elements defined as

$$\Theta_{kl}^{sc} = \langle U_kU_l + U_lU_k\rangle/2, \quad k, l = 1-8. \tag{9}$$

The verification of quantum entanglement via numerical simulation is key to quantum information science. In this section, we will demonstrate how to characterize quantum entanglement for continuous-variable systems.

Based on the Routh-Hurwitz criterion [64–67], the stability condition of the system can be found by letting all eigenvalues of the matrix $M_{\rm sc}$ have negative real parts. We consider the system in the stable case, in which the covariance matrix $\Theta_{\rm sc}$ fulfills the Lyapunov equation

$$M_{\rm sc}\Theta_{\rm sc} + \Theta_{\rm sc}M_{\rm sc}^T = -D, \tag{10}$$

where D is defined by

$$D_{kl}\delta(t-t') = \langle N_k(t)N_l(t') + N_l(t')N_k(t)\rangle/2. \tag{11}$$

By careful calculation, we found that D is a diagonal matrix ($j = 1, 2$),

$$D = \text{diag}[\kappa_a, \kappa_a, \kappa_j, \kappa_j, \gamma_b(2\bar{n}_b + 1), \gamma_b(2\bar{n}_b + 1)]. \quad (12)$$

For continuous-variable systems, it is appropriate to use logarithmic negativity to measure the magnitude of entanglement. To calculate the logarithmic negativity, we must identify each matrix element of the covariance matrix $\Theta_{\rm sc}$. Because the coefficient matrix $M_{\rm sc}$ and the diagonal matrix D are given in Eqs. (8) and (12), respectively, the covariance matrix $\Theta_{\rm sc}$ can be obtained directly by solving the Lyapunov equation (10). Then the bipartite entanglement between any pair of bosonic modes of the four-mode system can be calculated from the simplified 4×4 covariance matrix $\tilde{\Theta}_{\rm sc}$, which is extracted from the complete 8×8 covariance matrix $\Theta_{\rm sc}$ by keeping the corresponding mode components. When the dual-mode covariance submatrix $\tilde{\Theta}_{\rm sc}$ is expressed as

$$\tilde{\Theta}_{\rm sc} = \begin{pmatrix} \Xi_1 & \Xi_3 \\ \Xi_3^T & \Xi_2 \end{pmatrix}, \quad (13)$$

where Ξ_1, Ξ_2, and Ξ_3 are 2×2 block matrices, the bipartite entanglement described by the logarithmic negativity E_N is defined in the following form [57,59,64]:

$$E_N = \max[0, -\ln(2\mu_{\rm sc})], \quad (14)$$

where $\mu_{\rm sc} \equiv 2^{-1/2}\{\Pi_{\rm sc} - [\Pi_{\rm sc}^2 - 4\det\tilde{\Theta}_{\rm sc}]^{1/2}\}^{1/2}$ and $\Pi_{\rm sc} = \det\Xi_1 + \det\Xi_2 - 2\det\Xi_3$.

B. DC-ASA system dynamics

In this section, we study the steady-state dynamics of the DC-ASA magnomechanical system using an approach similar to that in Sec. III A and derive the logarithmic negativity of bipartite entanglement in the DC-ASA case.

Applying the QLEs and the typical linearization technique to the DC-ASA system, we then obtain the linearized Hamiltonian for the quantum fluctuation operators as follows:

$$H_{\rm dc}^{\rm lin} = H_{\rm sc}^{\rm lin} + J_2(\delta m_1^\dagger \delta m_2 + \delta m_1 \delta m_2^\dagger). \quad (15)$$

In the linearized system, we can study the steady-state dynamics of our dual-coupled model.

When $J_2 \neq 0$, the drift matrix $M_{\rm dc}$ of the DC-ASA system can be expressed as the sum of the single-coupled matrix $M_{\rm sc}$ and the matrix $\tilde{M}$ containing only the magnon-magnon coupling term J_2,

$$M_{\rm dc} = M_{\rm sc} + \tilde{M}, \quad (16)$$

where $\tilde{M}$ is given by

$$\tilde{M} = \begin{pmatrix} 0 & 0 & 0 & 0 & 0 & 0 & 0 & 0 \\ 0 & 0 & 0 & 0 & 0 & 0 & 0 & 0 \\ 0 & 0 & 0 & 0 & 0 & J_2 & 0 & 0 \\ 0 & 0 & 0 & 0 & -J_2 & 0 & 0 & 0 \\ 0 & 0 & 0 & J_2 & 0 & 0 & 0 & 0 \\ 0 & 0 & -J_2 & 0 & 0 & 0 & 0 & 0 \\ 0 & 0 & 0 & 0 & 0 & 0 & 0 & 0 \\ 0 & 0 & 0 & 0 & 0 & 0 & 0 & 0 \end{pmatrix}.$$

To obtain the information-related properties of the system, we need to specify the complete 8×8 covariance matrix $\Theta_{\rm dc}$. For a Gaussian state, the component of $\Theta_{\rm dc}$ can be represented by the vector U as

$$\Theta_{kl}^{\rm dc} = \langle U_k U_l + U_l U_k \rangle / 2, \quad k, l = 1 - 8. \quad (17)$$

In the steady-state case, the dynamics of the system will be governed by the Lyapunov equation

$$M_{\rm dc}\Theta_{\rm dc} + \Theta_{\rm dc} M_{\rm dc}^T = -D, \quad (18)$$

where D is the diffusion matrix which was given in Sec. III A. Numerically, the covariance matrix $\Theta_{\rm dc}$ can be obtained by directly solving Eq. (18). Using the matrix $\Theta_{\rm dc}$ obtained in the DC-ASA regime ($J_2 \neq 0$), we can numerically simulate the logarithmic negativity E_N of the bipartite entanglement as given in Eq. (14). Then, by comparing the result with the SC-ASA regime ($J_2 = 0$), we can observe the novel properties of bipartite entanglement under the DC-ASA effect.

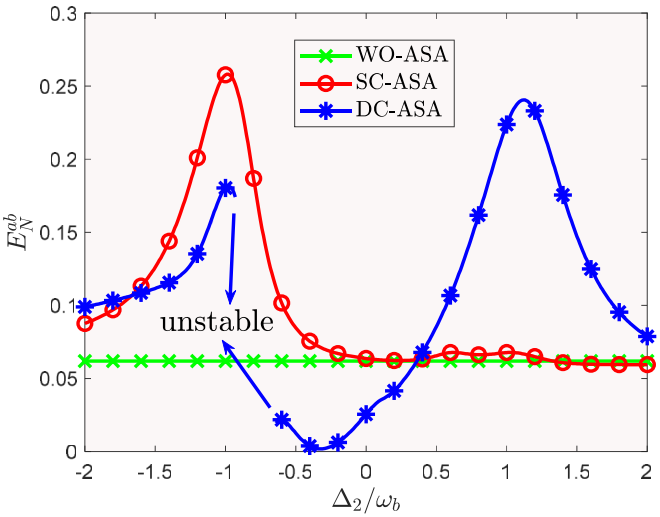

FIG. 3. Steady-state photon-phonon entanglement E_N^{ab} between the cavity mode δa and mechanical mode δb as a function of detuning Δ_2/ω_b for $J_1 = 0$ and $J_2 = 0$ (WO-ASA, green line with crosses), $J_1 = 0.32\omega_b$ and $J_2 = 0$ (SC-ASA, red line with circles), and $J_1 = 0.32\omega_b$ and $J_2 = 0.32\omega_b$ (DC-ASA, blue line with stars), where WO-ASA stands for "without auxiliary sphere assisted." The other parameters are $\omega_b/2\pi = 10$ MHz, $\Delta_a = -\omega_b$, $\Delta_1 = \omega_b$, $G_{am}/2\pi = G_{bm}/2\pi = 3.2$ MHz, $\kappa_a/2\pi = \kappa_1/2\pi = \kappa_2/2\pi = 1$ MHz, and $\gamma_b/2\pi = 100$ Hz. Here, we temporarily ignore the effect of mechanical thermal noise on entanglement (i.e., $\bar{n}_b = 0$), which will be discussed in detail in Fig. 8 in Sec. IV. The truncated part of the blue line indicates that the system is in an unstable region.

IV. RESULTS AND DISCUSSION

The ASA scheme can be applied to realize strong quantum entanglement between the optical mode δa and the mechanical mode δb. Now we study the properties of bipartite entanglement in the SC-ASA and DC-ASA regimes by numerically simulating the logarithmic negativity.

In Fig. 3, we show the steady-state cavity-oscillator entanglement E_N^{ab} versus the dimensionless detuning Δ_2/ω_b in the without auxiliary-sphere-assisted (WO-ASA), SC-ASA, and DC-ASA regimes. Here, we make the magnon mode δm_1 resonate with the blue sideband (i.e., $\Delta_1 = \omega_b$) and the cavity

mode δa resonate with the red sideband (i.e., $\Delta_a = -\omega_b$), which is a superior parameter regime for entanglement generation in a standard cavity magnomechanical system [18]. Clearly, E_N^{ab} reaches its maximum value at $\Delta_2/\omega_b \simeq -1$ ($\Delta_2/\omega_b \simeq 1$) in the SC-ASA (DC-ASA) regime, while it remains almost constant with increasing Δ_2/ω_b in the WO-ASA regime. For the SC-ASA mechanism, both the interaction terms J_1 and G_{bm} will be preserved in the rotating-wave approximation when $\Delta_2 = -\omega_b$, which means that both the optical mode δa and the mechanical mode δb can be cooled, and thus, the photon-phonon entanglement E_N^{ab} reaches its maximum. For the DC-ASA mechanism, although the J_1 term is discarded as a high-frequency oscillation term, the cooling effect of the J_2 and G_{bm} terms on the mechanical mode δb is optimal at $\Delta_2 = \omega_b$; thus, the maximum entanglement E_N^{ab} between photon δa and phonon δb is obtained when $\Delta_2 = \omega_b$. Moreover, the maximum value of E_N^{ab} is much larger in the case with ASA (SC-ASA and DC-ASA) than in the case without ASA (WO-ASA), which suggests that the ASA mechanism can, indeed, enhance entanglement. However, compared with the SC-ASA mechanism, the DC-ASA scheme does not further enhance the photon-phonon entanglement E_N^{ab} and drives the system to become unstable at $\Delta_2/\omega_b \simeq -1$, which is not in line with our expectation. We speculate that this is related to the symmetric magnetic dipole and magnetostrictive interactions (i.e., $G_{am} = G_{bm}$).

To verify our conjecture, we plot the cavity-oscillator bipartite entanglement E_N^{ab} versus the coupling ratio G_{am}/G_{bm} for $\Delta_2/\omega_b = 1$ [Fig. 4(a)] and $\Delta_2/\omega_b = -1$ [Fig. 4(b)]. When the system is under asymmetric magnetic dipole and magnetostrictive interactions (i.e., $G_{am} \neq G_{bm}$), especially, when $G_{am}/G_{bm} > 1$, the photon-phonon entanglement E_N^{ab} can be significantly enhanced by the SC-ASA [see the labeled red curve in Fig. 4(a)] and DC-ASA [see the labeled blue curve in Fig. 4(a)] methods. More interestingly, on the basis of the SC-ASA mechanism, E_N^{ab} can be significantly enhanced again via the DC-ASA method in Fig. 4(a), which is the result we want to see. At the same time, this confirms that our speculation is reasonable. In contrast to Fig. 4(a), E_N^{ab} is significantly reduced by the DC-ASA scheme compared to the SC-ASA mechanism in Fig. 4(b). But the maximum value of E_N^{ab} is smaller in the SC-ASA scenario in Fig. 4(b) than in the DC-ASA scenario in Fig. 4(a). And the stability of the system is highly susceptible to being destabilized with the increase of G_{am}/G_{bm} when the system works in both SC-ASA and DC-ASA regimes, as can be seen in Fig. 4(b). Therefore, below, we discard the case of $\Delta_2/\omega_b = -1$.

To get physical insight, we rewrite the linearized SC-ASA Hamiltonian (7) as

$$\begin{aligned} H_{\rm sc}^{sv} &= H_{\rm sc}^{fr} + H_{\rm sc}^{gc} + H_{\rm sc}^{js}, \\ H_{\rm sc}^{fr} &= \omega_b(\beta_{ba}^\dagger\beta_{ba} - \beta_{ab}^\dagger\beta_{ab} + \delta m_1^\dagger\delta m_1) + \Delta_2\delta m_2^\dagger\delta m_2, \\ H_{\rm sc}^{gc} &= G(\beta_{ab}^\dagger\delta m_1 + \beta_{ab}\delta m_1^\dagger) + \cosh r(\delta m_1^\dagger\beta_{ba} + \delta m_1\beta_{ba}^\dagger), \\ H_{\rm sc}^{js} &= J_1(\delta a^\dagger\delta m_2 + \delta a\delta m_2^\dagger) - \sinh r(\delta m_1\beta_{ab} + \delta m_1^\dagger\beta_{ab}^\dagger) \end{aligned} \tag{19}$$

by introducing two superposed Bogoliubov modes,

$$\beta_{ab} = \delta a\cosh r + \delta b^\dagger \sinh r \tag{20}$$

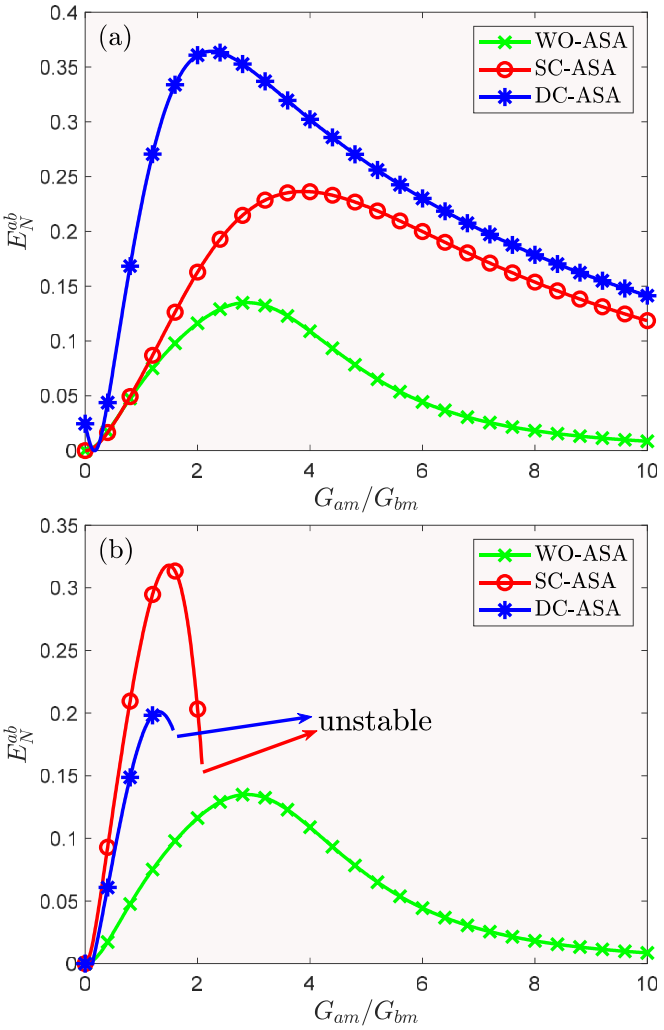

FIG. 4. Steady-state photon-phonon entanglement E_N^{ab} as a function of the coupling ratio G_{am}/G_{bm} for (a) $\Delta_2 = \omega_b$ and (b) $\Delta_2 = -\omega_b$ in the WO-ASA ($J_1 = 0$ and $J_2 = 0$, green line), SC-ASA ($J_1 = 0.32\omega_b$ and $J_2 = 0$, red line), and DC-ASA ($J_1 = 0.32\omega_b$ and $J_2 = 0.32\omega_b$, blue line) cases. The truncated part of the line represents the unstable regime. Other parameters are the same as those used in Fig. 3.

and

$$\beta_{ba} = \delta b\cosh r + \delta a^\dagger \sinh r, \tag{21}$$

where we have taken $\Delta_1 = -\Delta_a = \omega_b$, $r = \operatorname{arctanh}(G_{bm}/G_{am})$ is the squeezing parameter, and $G = \sqrt{G_{am}^2 - G_{bm}^2}$ is the effective coupling strength between the magnon mode δm_1 and the superposed mode β_{ab}. Similarly, the full Hamiltonian (15) of the DC-ASA system can be expressed in terms of the superposed Bogoliubov modes β_{ab} and β_{ba} as

$$H_{\rm dc}^{sv} = H_{\rm sc}^{sv} + J_2(\delta m_1^\dagger\delta m_2 + \delta m_1\delta m_2^\dagger). \tag{22}$$

Physically, the magnon mode δm_1 acts as a cold reservoir that can simultaneously cool the superposed Bogoliubov modes β_{ab} and β_{ba} via beam-splitter-type interactions $G(\beta_{ab}^\dagger\delta m_1 + \beta_{ab}\delta m_1^\dagger)$ and $\cosh r(\delta m_1^\dagger\beta_{ba} + \delta m_1\beta_{ba}^\dagger)$,

respectively, which can be found from the H_{sc}^{gc} term in Eq. (19). However, the parametric amplification interaction $\sinh r(\delta m_1 \beta_{ab} + \delta m_1^\dagger \beta_{ab}^\dagger)$ from the H_{sc}^{js} term in Eq. (19) suppresses the cooling of the superposed mode β_{ab}, which is detrimental for the enhancement of the cavity-oscillator entanglement E_N^{ab}. To eliminate the parametric amplification process for δm_1 and β_{ab}, we set $G \gg \sinh r$, which requires $G_{am} \gg G_{bm}$. For the general scheme [68,69], the dark mode β_{ba} is decoupled from the reservoir mode δm_1, and only the superposed mode β_{ab} can be cooled. However, we obtain a double-mode cooling effect for the superposed modes β_{ab} and β_{ba} by optimizing the coupling strength relation such that $G_{am} \gg G_{bm}$. Under the asymmetric coupling relation $G_{am} \gg G_{bm}$, the hybrid system can be rapidly cooled via the double-mode cooling effect, which drives the photon δa to be strongly entangled with the phonon δb. This well explains the quantum phenomenon in Fig. 4. Furthermore, the $J_1(\delta a^\dagger \delta m_2 + \delta a \delta m_2^\dagger)$ term in Eq. (19) indicates that the nonsuperposed mode δa can be cooled via the magnetostatic mode δm_2 containing the cooling rate J_1. Simultaneously, the auxiliary mode δm_2 acts as an additional cold bath that can efficiently cool the reservoir mode δm_1 via the dipolelike interaction $J_2(\delta m_1^\dagger \delta m_2 + \delta m_1 \delta m_2^\dagger)$ in Eq. (22). The double-mode cooling effect of δm_1 on the Bogoliubov modes β_{ab} and β_{ba} can operate more efficiently only if the thermal occupancy stored in the reservoir mode δm_1 is sustainably extracted from the cold environment δm_2.

Next, considering the asymmetric coupling regime $G_{am} = 2G_{bm}$, the steady-state occupancies $\langle \beta_{ab}^\dagger \beta_{ab} \rangle$ and $\langle \beta_{ba}^\dagger \beta_{ba} \rangle$ of the superposed modes β_{ab} and β_{ba} are shown in Fig. 5 and are expressed as

$$\langle \beta_{ab}^\dagger \beta_{ab} \rangle = \cosh^2 r \Lambda_a + \sinh^2 r(\Lambda_b + 1) + \tfrac{1}{2} \sinh 2r \Lambda_{a+b} \tag{23}$$

and

$$\langle \beta_{ba}^\dagger \beta_{ba} \rangle = \cosh^2 r \Lambda_b + \sinh^2 r(\Lambda_a + 1) + \tfrac{1}{2} \sinh 2r \Lambda_{a+b}, \tag{24}$$

with

$$\Lambda_a = \langle \delta a^\dagger \delta a \rangle,\ \Lambda_b = \langle \delta b^\dagger \delta b \rangle,\ \Lambda_{a+b} = \langle \delta a^\dagger \delta b^\dagger + \delta a \delta b \rangle.$$

In Fig. 5(a), we show the steady-state occupation $\langle \beta_{ab}^\dagger \beta_{ab} \rangle$ as a function of the effective detuning Δ_2/ω_b for $J_1 = 0$ and $J_2 = 0$ (green curve with crosses), $J_1 = 0.32\omega_b$ and $J_2 = 0$ (red curve with circles), and $J_1 = 0.32\omega_b$ and $J_2 = 0.32\omega_b$ (blue curve with stars). As a whole, the steady-state occupancy $\langle \beta_{ab}^\dagger \beta_{ab} \rangle$ remains almost constant (unaffected) for the WO-ASA case. In the SC-ASA regime, the sudden enhancement of the occupation $\langle \beta_{ab}^\dagger \beta_{ab} \rangle$ at $\Delta_2/\omega_b \simeq -1$ is due to the fact that the $J_1(\delta a^\dagger \delta m_2 + \delta a \delta m_2^\dagger)$ term in Eq. (19) cannot be discarded under the rotating-wave approximation $\Delta_a = -\omega_b$ and $\Delta_2 = -\omega_b$. As a result, only the optical mode δa in the superposed mode β_{ab} can be cooled via the interaction J_1, while the mechanical mode δb cannot be cooled, which leads to the superposed mode β_{ab} itself becoming unbalanced. When the system is operated in the DC-ASA regime, the steady-state occupancy $\langle \beta_{ab}^\dagger \beta_{ab} \rangle$ also tends to grow significantly, and the system becomes unstable at $\Delta_2/\omega_b \simeq -1$. This is due to the fact that the beam-splitter interaction

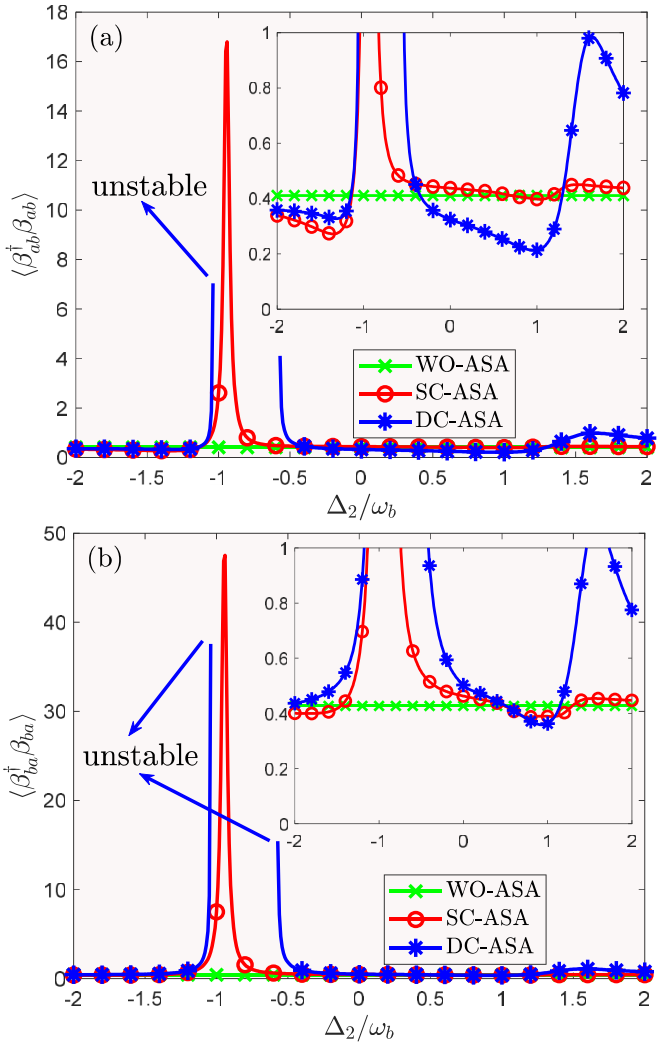

FIG. 5. Steady-state occupancies of the superposed modes (a) $\langle \beta_{ab}^\dagger \beta_{ab} \rangle$ and (b) $\langle \beta_{ba}^\dagger \beta_{ba} \rangle$ versus the dimensionless detuning Δ_2/ω_b with $G_{am} = 2G_{bm}$ in the WO-ASA ($J_1 = J_2 = 0$, green line), SC-ASA ($J_1 = 0.32\omega_b$ and $J_2 = 0$, red line), and DC-ASA ($J_1 = J_2 = 0.32\omega_b$, blue line) cases. The truncated part of the line denotes the unstable regime. Other parameters are the same as those used in Fig. 3.

$J_2(\delta m_1^\dagger \delta m_2 + \delta m_1 \delta m_2^\dagger)$ between the deformed sphere δm_1 and the auxiliary sphere δm_2 in Eq. (22) can be safely neglected when the rotating-wave approximation condition $J_2 \ll 2\omega_b$ is satisfied for $J_2 = 0.32\omega_b$ with $\Delta_1 = \omega_b$ and $\Delta_2 = -\omega_b$, and therefore, the reservoir mode δm_1 cannot be efficiently cooled. Physically, the thermal excitations stored in the reservoir mode δm_1 cannot be efficiently extracted from the cold bath δm_2, which inhibits the rapid cooling process between modes δm_1 and β_{ab}. As a result, the steady-state occupancy $\langle \beta_{ab}^\dagger \beta_{ab} \rangle$ is large, and the system is susceptible to becoming unstable via thermal perturbations.

Locally, when $\Delta_2/\omega_b = 1$, the cooling of the superposed mode β_{ab} can be improved by opening only the SC-ASA channel, but it can be further significantly enhanced by switching the DC-ASA passage, as shown in the inset of Fig. 5(a).

Physically, the cooling process of the magnomechanical system can be accelerated by utilizing the DC-ASA method. This study provides a simple scheme for improving the cooling limit of the bosonic modes by using only an additional auxiliary sphere. By choosing the two-mode cooling parameter $G_{am} = 2G_{bm}$, the occupancy $\langle \beta_{ba}^{\dagger}\beta_{ba}\rangle$ exhibits a dynamic behavior similar to that of $\langle \beta_{ab}^{\dagger}\beta_{ab}\rangle$, as can be seen in Fig. 5(b). Differently, in the DC-ASA regime, the optimal value of the steady-state occupation $\langle \beta_{ab}^{\dagger}\beta_{ab}\rangle$ ($\langle \beta_{ab}^{\dagger}\beta_{ab}\rangle \simeq 0.21$) is superior to that of $\langle \beta_{ba}^{\dagger}\beta_{ba}\rangle$ ($\langle \beta_{ba}^{\dagger}\beta_{ba}\rangle \simeq 0.36$) at $\Delta_2/\omega_b \simeq 1$, as can be clearly seen in the insets of Figs. 5(a) and 5(b). This is attributed to the fact that the coupling rate G between the reservoir mode δm_1 and the superposed mode β_{ab} is stronger than the cooling rate $\cosh r$ between modes δm_1 and β_{ba} when $G_{am} = 2G_{bm}$.

Figure 5 again demonstrates that the detuning parameter $\Delta_2 = -\omega_b$ destabilizes the system. Therefore, choosing a reasonable parameter regime $\Delta_2 = \omega_b$, we plot the steady-state occupancies $\langle \beta_{ab}^{\dagger}\beta_{ab}\rangle$ and $\langle \beta_{ba}^{\dagger}\beta_{ba}\rangle$ as a function of the effective coupling ratio G_{am}/G_{bm} for the WO-ASA ($J_1 = 0$, $J_2 = 0$), SC-ASA ($J_1 = 0.32\omega_b$, $J_2 = 0$), and DC-ASA ($J_1 = 0.32\omega_b$, $J_2 = 0.32\omega_b$) regimes in Figs. 6(a) and 6(b), respectively. Interestingly, the superposed mode β_{ab} undergoes a "quantum quenching" phenomenon when the ratio G_{am}/G_{bm} varies approximately from 1 to 1.2; i.e., the occupancy $\langle \beta_{ab}^{\dagger}\beta_{ab}\rangle$ decreases sharply over a very small parameter interval $G_{am}/G_{bm} \in [1, 1.2]$ for the above three mechanisms. It is easy to understand that according to Eq. (19), the cooling process between the reservoir mode δm_1 and the superposed mode β_{ab} is weaker than the parametric process between them when $G_{am} \simeq G_{bm}$ (i.e., $G = \sqrt{G_{am}^2 - G_{bm}^2} \ll \sinh r$), and therefore, the Bogoliubov mode β_{ab} cannot be cooled efficiently. However, as G_{am}/G_{bm} increases, the cooling process between δm_1 and β_{ab} becomes progressively stronger than the heating process between them, so β_{ab} can be efficiently cooled by the cold reservoir δm_1. In particular, when $G_{am}/G_{bm} > 2$, with a further increase of G_{am}/G_{bm} ($G_{am}/G_{bm} \to 10$) the Bogoliubov mode β_{ab} gradually approaches its quantum ground state ($\langle \beta_{ab}^{\dagger}\beta_{ab}\rangle \to 0$), which can be clearly seen from the inset of Fig. 6(a). More importantly, in the inset of Fig. 6(a), the cooling of the superposed mode β_{ab} can be enhanced by opening the SC-ASA channel compared to the WO-ASA case, and the occupancy $\langle \beta_{ab}^{\dagger}\beta_{ab}\rangle$ can be significantly reduced again when the DC-ASA passage is opened. In the DC-ASA mechanism, both the nonsuperposed mode δa and the reservoir mode δm_1 can be cooled by an additional cold bath δm_2 compared to the SC-ASA approach, which accelerates the cooling process of β_{ab}.

In Fig. 6(b), the occupancy $\langle \beta_{ba}^{\dagger}\beta_{ba}\rangle$ of β_{ba} exhibits almost the same trend with G_{am}/G_{bm} evolution as $\langle \beta_{ab}^{\dagger}\beta_{ab}\rangle$. It should be mentioned that when the ratio G_{am}/G_{bm} is approximately in the interval $G_{am}/G_{bm} \in [3, 10]$, the cooling effect of β_{ab} is better than that of β_{ba} for the WO-ASA, SC-ASA, and DC-ASA regimes [see insets in Figs. 6(a) and 6(b)]. The reason for this phenomenon was explained in the discussion of Fig. 5. Moreover, from the green line with crosses in the inset of Fig. 6(b) we find that the occupancy $\langle \beta_{ba}^{\dagger}\beta_{ba}\rangle$ will be monotonically increasing when G_{am}/G_{bm} is approximately greater than 3. This is due to the fact that thermal excitations

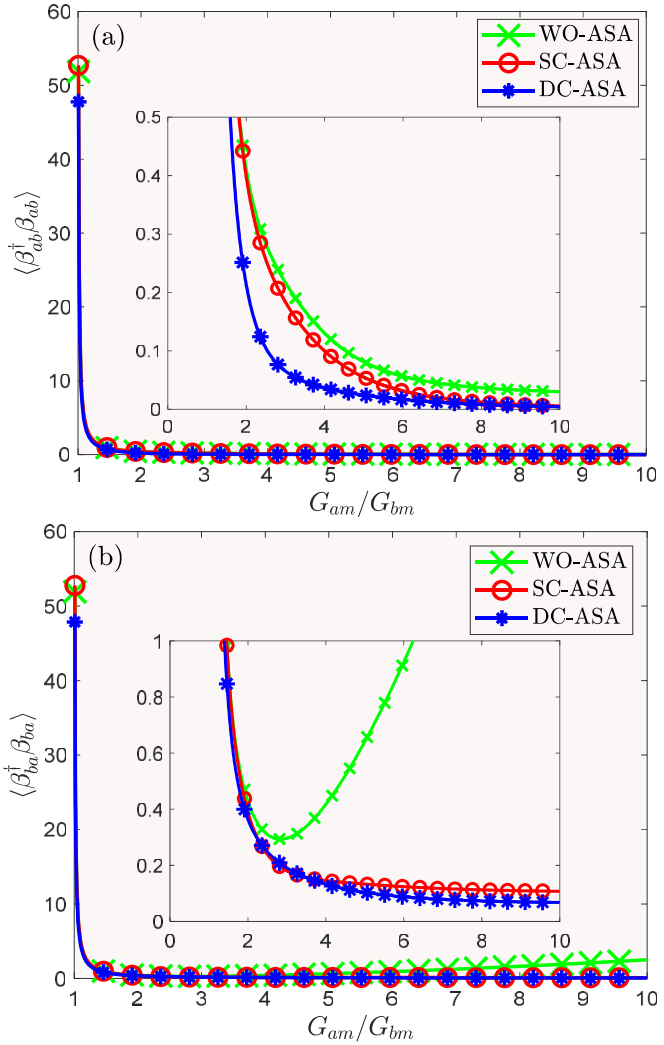

FIG. 6. Steady-state occupancies of the superposed modes (a) $\langle \beta_{ab}^{\dagger}\beta_{ab}\rangle$ and (b) $\langle \beta_{ba}^{\dagger}\beta_{ba}\rangle$ versus the ratio of the effective couplings G_{am}/G_{bm} for $J_1 = J_2 = 0$ (WO-ASA, green line with crosses), $J_1 = 0.32\omega_b$ and $J_2 = 0$ (SC-ASA, red line with circles), and $J_1 = J_2 = 0.32\omega_b$ (DC-ASA, blue line with stars). Here, $\Delta_2 = \omega_b$, and the other parameters are the same as those used in Fig. 3.

stored in the system in the case of WO-ASA cannot diffuse into the auxiliary environment, so the system becomes unstable as G_{am}/G_{bm} increases.

To find the optimal parametric conditions for cavity-resonator entanglement E_N^{ab}, we show the density plot of E_N^{ab} versus the dimensionless detuning Δ_2/ω_b and the ratio G_{am}/G_{bm} in the WO-ASA, SC-ASA, and DC-ASA regimes in Fig. 7. Compared to the WO-ASA case, the photon-phonon entanglement E_N^{ab} can be significantly improved by opening the SC-ASA channel. Remarkably, E_N^{ab} can be further significantly enhanced when we switch the coupling mechanism of the system from the SC-ASA passage to the DC-ASA channel, which is interesting. In the DC-ASA mechanism, not only the localized mode δa but also the reservoir mode δm_1 can be cooled via the auxiliary mode δm_2, which facilitates the enhancement of the photon-phonon entanglement E_N^{ab}. The white regions in Figs. 7(b) and 7(c) indicate that the system

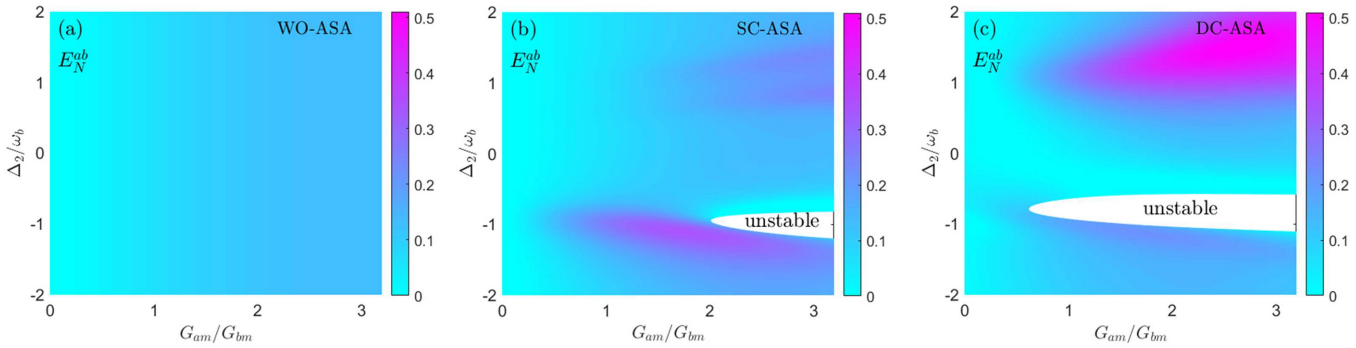

FIG. 7. Steady-state photon-phonon entanglement E_N^{ab} as a function of the dimensionless detuning Δ_2/ω_b and the ratio G_{am}/G_{bm} for (a) WO-ASA ($J_1 = J_2 = 0$), (b) SC-ASA ($J_1 = 0.32\omega_b$, $J_2 = 0$), and (c) DC-ASA ($J_1 = J_2 = 0.32\omega_b$). Other parameters are the same as those used in Fig. 3. The white areas in the density plots in (b) and (c) correspond to the instability of the system.

is in an unstable state. When the system works in the DC-ASA regime, the photon-phonon entanglement E_N^{ab} reaches its optimal value $E_N^{ab} \simeq 0.51$ in the approximate parameter space $1 < \Delta_2/\omega_b < 2$, $1.5 < G_{am}/G_{bm} < 3.2$ [see Fig. 7(c)]. Moreover, the maximum value of E_N^{ab} obtained with our DC-ASA scheme is about 2.5 times greater than that obtained in a standard cavity magnomechanical system [18].

By picking the optimal parameters $\Delta_2 = 1.35\omega_b$ and $G_{am} = 2.8G_{bm}$ based on Fig. 7(c), we plot the steady-state cavity-resonator entanglement E_N^{ab} as a function of the mean thermal occupancy $\bar{n}_b$ of the mechanical mode δb for $G_{am}/G_{bm} = 0.5$, $G_{am}/G_{bm} = 1$, and $G_{am}/G_{bm} = 2.8$ in Figs. 8(a)–8(c), respectively. When $G_{am} = 2.8G_{bm}$, the two-mode cooling conditions $G \gg \sinh r$ and $\cosh r > \sinh r$ hold, and thus, the superposed modes β_{ab} and β_{ba} can be cooled simultaneously via the interactions $G(\beta_{ab}^{\dagger}\delta m_1 + \beta_{ab}\delta m_1^{\dagger})$ and $\cosh r(\delta m_1^{\dagger}\beta_{ba} + \delta m_1\beta_{ba}^{\dagger})$, respectively, where δm_1 plays the role of a cold reservoir. With the double-mode cooling effect, β_{ab} and β_{ba} are cooled down to close to the quantum ground state, and we can achieve large steady-state entanglement between the cavity mode δa and the mechanical mode δb [see Fig. 8(c)]. As a comparison, for $G_{am} \leqslant G_{bm}$, the two-mode cooling conditions $G \gg \sinh r$ and $\cosh r > \sinh r$ are no longer satisfied, and thus, the photon-phonon entanglement E_N^{ab} is small [see Figs. 8(a) and 8(b)]. On the other hand, both E_N^{ab} and its robustness against the average thermal phonon $\bar{n}_b$ can be significantly enhanced by sequentially opening the SC-ASA and DC-ASA channels on the basis of the double-mode cooling effect. In particular, in the DC-ASA regime, E_N^{ab} can reach $E_N^{ab} \simeq 0.5$ and can survive even at the thermal occupancy $\bar{n}_b \simeq 10^4$, which corresponds to a thermal temperature $T \simeq 4.8$ K [see the blue curve with stars in Fig. 8(c)]. Physically, these findings provide a feasible approach for realizing strong and temperature-resistant quantum entanglement simply by switching the dual-coupling channel between the auxiliary system and the standard cavity magnomechanical system.

V. CONCLUSION

In summary, we designed a coupled cavity magnomechanical device with a deformed sphere, an auxiliary sphere, and a microwave cavity, where the auxiliary sphere is coupled to the microwave field via the magnetic dipole interaction and coupled to the deformed sphere by the tunable dipolelike interaction. Moreover, the mechanical oscillator induced by the deformed sphere interacts with the magnon mode of the deformed sphere via a magnetostrictive force and with the microwave cavity via a magnetic dipole coupling. By optimizing the beam-splitter interaction G and the parametric amplification interaction $\sinh r$ such that $G \gg \sinh r$, we can simultaneously cool the pair of superposed Bogoliubov modes

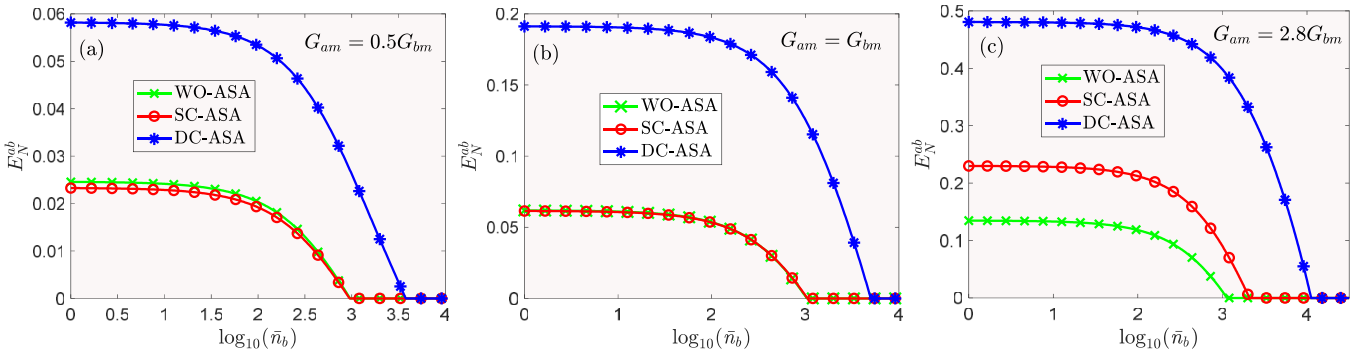

FIG. 8. Steady-state photon-phonon entanglement E_N^{ab} versus the logarithm $\log_{10}(\bar{n}_b)$ of the average thermal occupancy $\bar{n}_b$ of the mechanical mode δb for (a) $G_{am} = 0.5G_{bm}$, (b) $G_{am} = G_{bm}$, and (c) $G_{am} = 2.8G_{bm}$. Here, $\Delta_2 = 1.35\omega_b$, and the other parameters are the same as those used in Fig. 3.

β_{ab} and β_{ba} through the reservoir mode. The steady-state photon-phonon entanglement is strong under the double-mode cooling parameters. And the photon-phonon entanglement can be significantly enhanced by opening the SC-ASA channel compared with the case without the auxiliary sphere, which is due to the fact that the nonsuperposed optical mode can be efficiently cooled via the single-coupling between the auxiliary sphere and the microwave cavity. More interestingly, the photon-phonon entanglement on the basis of the SC-ASA mechanism can be significantly improved again by switching the DC-ASA passage, where both the nonsuperposed cavity mode and the reservoir mode can be cooled by the dual-coupling between the auxiliary sphere and the standard magnomechanical system. Our numerical results also show that the steady-state cavity-vibrator entanglement can survive at higher thermal temperatures in the DC-ASA regime. This DC-ASA approach provides a promising platform for the preparation of strongly squeezed states and enhanced magnomechanical cooling.

ACKNOWLEDGMENTS

This work was supported by the National Natural Science Foundation of China (Grants No. 11874190 and No. 12247101). Support was also provided by the Supercomputing Center of Lanzhou University.

[1] L. Bai, M. Harder, Y. P. Chen, X. Fan, J. Q. Xiao, and C.-M. Hu, Spin pumping in electrodynamically coupled magnon-photon systems, Phys. Rev. Lett. **114**, 227201 (2015).

[2] J. Bourhill, N. Kostylev, M. Goryachev, D. L. Creedon, and M. E. Tobar, Ultrahigh cooperativity interactions between magnons and resonant photons in a YIG sphere, Phys. Rev. B **93**, 144420 (2016).

[3] N. Kostylev, M. Goryachev, and M. E. Tobar, Superstrong coupling of a microwave cavity to yttrium iron garnet magnons, Appl. Phys. Lett. **108**, 062402 (2016).

[4] R. Hisatomi, A. Osada, Y. Tabuchi, T. Ishikawa, A. Noguchi, R. Yamazaki, K. Usami, and Y. Nakamura, Bidirectional conversion between microwave and light via ferromagnetic magnons, Phys. Rev. B **93**, 174427 (2016).

[5] A. Osada, R. Hisatomi, A. Noguchi, Y. Tabuchi, R. Yamazaki, K. Usami, M. Sadgrove, R. Yalla, M. Nomura, and Y. Nakamura, Cavity optomagnonics with spin-orbit coupled photons, Phys. Rev. Lett. **116**, 223601 (2016).

[6] X. Zhang, N. Zhu, C.-L. Zou, and H. X. Tang, Optomagnonic whispering gallery microresonators, Phys. Rev. Lett. **117**, 123605 (2016).

[7] J. A. Haigh, A. Nunnenkamp, A. J. Ramsay, and A. J. Ferguson, Triple-resonant Brillouin light scattering in magneto-optical cavities, Phys. Rev. Lett. **117**, 133602 (2016).

[8] S. Viola Kusminskiy, H. X. Tang, and F. Marquardt, Coupled spin-light dynamics in cavity optomagnonics, Phys. Rev. A **94**, 033821 (2016).

[9] S. Sharma, Y. M. Blanter, and G. E. W. Bauer, Light scattering by magnons in whispering gallery mode cavities, Phys. Rev. B **96**, 094412 (2017).

[10] A. Osada, A. Gloppe, Y. Nakamura, and K. Usami, Orbital angular momentum conservation in Brillouin light scattering within a ferromagnetic sphere, New J. Phys. **20**, 103018 (2018).

[11] A. Osada, A. Gloppe, R. Hisatomi, A. Noguchi, R. Yamazaki, M. Nomura, Y. Nakamura, and K. Usami, Brillouin light scattering by magnetic quasivortices in cavity optomagnonics, Phys. Rev. Lett. **120**, 133602 (2018).

[12] H. Huebl, C. W. Zollitsch, J. Lotze, F. Hocke, M. Greifenstein, A. Marx, R. Gross, and S. T. B. Goennenwein, High cooperativity in coupled microwave resonator ferrimagnetic insulator hybrids, Phys. Rev. Lett. **111**, 127003 (2013).

[13] Y. Tabuchi, S. Ishino, T. Ishikawa, R. Yamazaki, K. Usami, and Y. Nakamura, Hybridizing ferromagnetic magnons and microwave photons in the quantum limit, Phys. Rev. Lett. **113**, 083603 (2014).

[14] M. Goryachev, W. G. Farr, D. L. Creedon, Y. Fan, M. Kostylev, and M. E. Tobar, High-cooperativity cavity QED with magnons at microwave frequencies, Phys. Rev. Appl. **2**, 054002 (2014).

[15] X. Zhang, C.-L. Zou, L. Jiang, and H. X. Tang, Strongly coupled magnons and cavity microwave photons, Phys. Rev. Lett. **113**, 156401 (2014).

[16] Y. Tabuchi, S. Ishino, A. Noguchi, T. Ishikawa, R. Yamazaki, K. Usami, and Y. Nakamura, Quantum magnonics: The magnon meets the superconducting qubit, C. R. Phys. **17**, 729 (2016).

[17] X. Zhang, C.-L. Zou, L. Jiang, and H. X. Tang, Cavity magnomechanics, Sci. Adv. **2**, e1501286 (2016).

[18] J. Li, S.-Y. Zhu, and G. S. Agarwal, Magnon-photon-phonon entanglement in cavity magnomechanics, Phys. Rev. Lett. **121**, 203601 (2018).

[19] K. Ullah, M. T. Naseem, and Ö. E. Müstecaplıoğlu, Tunable multiwindow magnomechanically induced transparency, Fano resonances, and slow-to-fast light conversion, Phys. Rev. A **102**, 033721 (2020).

[20] B. Wang, Z.-X. Liu, C. Kong, H. Xiong, and Y. Wu, Magnon-induced transparency and amplification in $\mathcal{PT}$-symmetric cavity-magnon system, Opt. Express **26**, 20248 (2018).

[21] Y.-P. Wang, G.-Q. Zhang, D. Zhang, T.-F. Li, C.-M. Hu, and J. Q. You, Bistability of cavity magnon polaritons, Phys. Rev. Lett. **120**, 057202 (2018).

[22] D. Zhang, X.-M. Wang, T.-F. Li, X.-Q. Luo, W. Wu, F. Nori, and J. Q. You, Cavity quantum electrodynamics with ferromagnetic magnons in a small yttrium-iron-garnet sphere, npj Quantum Inf. **1**, 15014 (2015).

[23] Y.-P. Wang, J. W. Rao, Y. Yang, P.-C. Xu, Y. S. Gui, B. M. Yao, J. Q. You, and C.-M. Hu, Nonreciprocity and unidirectional invisibility in cavity magnonics, Phys. Rev. Lett. **123**, 127202 (2019).

[24] Y. Iguchi, S. Uemura, K. Ueno, and Y. Onose, Nonreciprocal magnon propagation in a noncentrosymmetric ferromagnet Li, Phys. Rev. B **92**, 184419 (2015).

[25] C. Kong, H. Xiong, and Y. Wu, Magnon-induced nonreciprocity based on the magnon Kerr effect, Phys. Rev. Appl. **12**, 034001 (2019).

[26] Z. Zhang, M. O. Scully, and G. S. Agarwal, Quantum entanglement between two magnon modes via Kerr nonlinearity driven far from equilibrium, Phys. Rev. Res. **1**, 023021 (2019).

[27] R.-C. Shen, Y.-P. Wang, J. Li, S.-Y. Zhu, G. S. Agarwal, and J. Q. You, Long-time memory and ternary logic gate using a multistable cavity magnonic system, Phys. Rev. Lett. **127**, 183202 (2021).

[28] Z.-X. Liu, H. Xiong, and Y. Wu, Room-temperature slow light in a coupled cavity magnon-photon system, IEEE Access **7**, 57047 (2019).

[29] C. Kong, B. Wang, Z.-X. Liu, H. Xiong, and Y. Wu, Magnetically controllable slow light based on magnetostrictive forces, Opt. Express **27**, 5544 (2019).

[30] X. Li, W.-X. Yang, T. Shui, L. Li, X. Wang, and Z. Wu, Phase control of the transmission in cavity magnomechanical system with magnon driving, J. Appl. Phys. **128**, 233101 (2020).

[31] F. Wang, C. Gou, J. Xu, and C. Gong, Hybrid magnon-atom entanglement and magnon blockade via quantum interference, Phys. Rev. A **106**, 013705 (2022).

[32] Z.-X. Liu, H. Xiong, and Y. Wu, Magnon blockade in a hybrid ferromagnet-superconductor quantum system, Phys. Rev. B **100**, 134421 (2019).

[33] J.-K. Xie, S.-L. Ma, and F.-L. Li, Quantum-interference-enhanced magnon blockade in an yttrium-iron-garnet sphere coupled to superconducting circuits, Phys. Rev. A **101**, 042331 (2020).

[34] Y.-J. Xu, T.-L. Yang, L. Lin, and J. Song, Conventional and unconventional magnon blockades in a qubit-magnon hybrid quantum system, J. Opt. Soc. Am. B **38**, 876 (2021).

[35] C. Zhao, X. Li, S. Chao, R. Peng, C. Li, and L. Zhou, Simultaneous blockade of a photon, phonon, and magnon induced by a two-level atom, Phys. Rev. A **101**, 063838 (2020).

[36] K. Wu, W.-X. Zhong, G.-L. Cheng, and A.-X. Chen, Phase-controlled multimagnon blockade and magnon-induced tunneling in a hybrid superconducting system, Phys. Rev. A **103**, 052411 (2021).

[37] M.-S. Ding, L. Zheng, and C. Li, Ground-state cooling of a magnomechanical resonator induced by magnetic damping, J. Opt. Soc. Am. B **37**, 627 (2020).

[38] Z.-X. Yang, L. Wang, Y.-M. Liu, D.-Y. Wang, C.-H. Bai, S. Zhang, and H.-F. Wang, Ground state cooling of magnomechanical resonator in $\mathcal{PT}$-symmetric cavity magnomechanical system at room temperature, Front. Phys. **15**, 52504 (2020).

[39] Z. Yang, C. Zhao, R. Peng, J. Yang, and L. Zhou, Improving mechanical cooling by using magnetic thermal noise in a cavity-magnomechanical system, Opt. Lett. **48**, 375 (2023).

[40] A. Kani, B. Sarma, and J. Twamley, Intensive cavity-magnomechanical cooling of a levitated macromagnet, Phys. Rev. Lett. **128**, 013602 (2022).

[41] W. Qiu, X. Cheng, A. Chen, Y. Lan, and W. Nie, Controlling quantum coherence and entanglement in cavity magnomechanical systems, Phys. Rev. A **105**, 063718 (2022).

[42] Y.-T. Chen, L. Du, Y. Zhang, and J.-H. Wu, Perfect transfer of enhanced entanglement and asymmetric steering in a cavity-magnomechanical system, Phys. Rev. A **103**, 053712 (2021).

[43] J. Li, S.-Y. Zhu, and G. S. Agarwal, Squeezed states of magnons and phonons in cavity magnomechanics, Phys. Rev. A **99**, 021801(R) (2019).

[44] Q. Guo, J. Cheng, H. Tan, and J. Li, Magnon squeezing by two-tone driving of a qubit in cavity-magnon-qubit systems, Phys. Rev. A **108**, 063703 (2023).

[45] T.-X. Lu, X. Xiao, L.-S. Chen, Q. Zhang, and H. Jing, Magnon-squeezing-enhanced slow light and second-order sideband in cavity magnomechanics, Phys. Rev. A **107**, 063714 (2023).

[46] S. Chakraborty and C. Das, Nonreciprocal magnon-photon-phonon entanglement in cavity magnomechanics, Phys. Rev. A **108**, 063704 (2023).

[47] Z.-Y. Fan, H. Qian, X. Zuo, and J. Li, Entangling ferrimagnetic magnons with an atomic ensemble via optomagnomechanics, Phys. Rev. A **108**, 023501 (2023).

[48] Y. Wu, J.-H. Liu, Y.-F. Yu, Z.-M. Zhang, and J.-D. Wang, Entangling a magnon and an atomic ensemble mediated by an optical cavity, Phys. Rev. Appl. **20**, 034043 (2023).

[49] M. Yu, H. Shen, and J. Li, Magnetostrictively induced stationary entanglement between two microwave fields, Phys. Rev. Lett. **124**, 213604 (2020).

[50] H. Tan and J. Li, Einstein-Podolsky-Rosen entanglement and asymmetric steering between distant macroscopic mechanical and magnonic systems, Phys. Rev. Res. **3**, 013192 (2021).

[51] J.-X. Han, J.-L. Wu, Y. Wang, Y. Xia, Y.-Y. Jiang, and J. Song, Tripartite high-dimensional magnon-photon entanglement in phases with broken $\mathcal{PT}$-symmetry of a non-Hermitian hybrid system, Phys. Rev. B **105**, 064431 (2022).

[52] Z.-B. Yang, W.-J. Wu, J. Li, Y.-P. Wang, and J. Q. You, Steady-entangled-state generation via the cross-Kerr effect in a ferrimagnetic crystal, Phys. Rev. A **106**, 012419 (2022).

[53] D.-W. Luo, X.-F. Qian, and T. Yu, Nonlocal magnon entanglement generation in coupled hybrid cavity systems, Opt. Lett. **46**, 1073 (2021).

[54] Y.-L. Ren, J.-K. Xie, X.-K. Li, S.-L. Ma, and F.-L. Li, Long-range generation of a magnon-magnon entangled state, Phys. Rev. B **105**, 094422 (2022).

[55] Z.-B. Yang, J.-S. Liu, H. Jin, Q.-H. Zhu, A.-D. Zhu, H.-Y. Liu, Y. Ming, and R.-C. Yang, Entanglement enhanced by Kerr nonlinearity in a cavity-optomagnonics system, Opt. Express **28**, 31862 (2020).

[56] L.-J. Cong, Y.-X. Luo, Z.-G. Zheng, H.-Y. Liu, Y. Ming, and R.-C. Yang, Entanglement generation and steering implementation in a double-cavity-magnon hybrid system, Opt. Express **31**, 34021 (2023).

[57] Z.-Q. Liu, Y. Liu, L. Tan, and W.-M. Liu, Reservoir engineering strong magnomechanical entanglement via dual-mode cooling, Ann. Phys. (Berlin, Ger.) **535**, 2200660 (2023).

[58] B. Hussain, S. Qamar, and M. Irfan, Entanglement enhancement in cavity magnomechanics by an optical parametric amplifier, Phys. Rev. A **105**, 063704 (2022).

[59] Z.-Q. Liu, L. Liu, Z.-Z. Meng, L. Tan, and W.-M. Liu, Simultaneously enhanced magnomechanical cooling and entanglement assisted by an auxiliary microwave cavity, Opt. Express **32**, 722 (2024).

[60] M. Amazioug, B. Teklu, and M. Asjad, Enhancement of magnonphotonphonon entanglement in a cavity magnomechanics with coherent feedback loop, Sci. Rep. **13**, 3833 (2023).

[61] D.-G. Lai, W. Qin, B.-P. Hou, A. Miranowicz, and F. Nori, Significant enhancement in refrigeration and entanglement in auxiliary-cavity-assisted optomechanical systems, Phys. Rev. A **104**, 043521 (2021).

[62] J.-S. Feng, L. Tan, H.-Q. Gu, and W.-M. Liu, Auxiliary-cavity-assisted ground-state cooling of an optically levitated

nanosphere in the unresolved-sideband regime, Phys. Rev. A **96**, 063818 (2017).

[63] N. Crescini, C. Braggio, G. Carugno, A. Ortolan, and G. Ruoso, Coherent coupling between multiple ferrimagnetic spheres and a microwave cavity at millikelvin temperatures, Phys. Rev. B **104**, 064426 (2021).

[64] D. Vitali, S. Gigan, A. Ferreira, H. R. Böhm, P. Tombesi, A. Guerreiro, V. Vedral, A. Zeilinger, and M. Aspelmeyer, Optomechanical entanglement between a movable mirror and a cavity field, Phys. Rev. Lett. **98**, 030405 (2007).

[65] E. X. DeJesus and C. Kaufman, Routh-Hurwitz criterion in the examination of eigenvalues of a system of nonlinear ordinary differential equations, Phys. Rev. A **35**, 5288 (1987).

[66] L.-M. Duan, G. Giedke, J. I. Cirac, and P. Zoller, Inseparability criterion for continuous variable systems, Phys. Rev. Lett. **84**, 2722 (2000).

[67] M. Paternostro, D. Vitali, S. Gigan, M. S. Kim, C. Brukner, J. Eisert, and M. Aspelmeyer, Creating and probing multipartite macroscopic entanglement with light, Phys. Rev. Lett. **99**, 250401 (2007).

[68] R.-X. Chen, L.-T. Shen, and S.-B. Zheng, Dissipation-induced optomechanical entanglement with the assistance of Coulomb interaction, Phys. Rev. A **91**, 022326 (2015).

[69] Y.-D. Wang and A. A. Clerk, Reservoir-engineered entanglement in optomechanical systems, Phys. Rev. Lett. **110**, 253601 (2013).